UNCONVENTIONAL RESOURCES TECHNOLOGY CONFERENCE
URTeC

URTeC: 4266460

An Integrated Experimental and Molecular Dynamics Simulation Study to Investigate the Impact of Nanofluidic Phenomena on CO_2 Huff-n-Puff Results in Unconventional Reservoirs

Dina Hegazy[1], Huajie Zhang,[3] Xiaolong Yin[1,2], Rui Qiao[3], Erdal Ozkan[1], 1. Colorado School of Mines, 2. Eastern Institute of Technology, 3. Virginia Polytechnic Institute and State University.

This paper was prepared for presentation at the Unconventional Resources Technology Conference held in Houston, Texas, USA, 9-11 June 2025.

Abstract

Unconventional reservoirs are dominated by nanopores, where the flow of interfacial fluids is significantly influenced by confinement and interfacial forces. However, nanofluidic physics is not usually considered in classic hydrodynamics and incorporated into conventional reservoir simulators. This study explores the nanofluidic physics of oil and CO_2 transport arising from CO_2 and its gradient at oil-wall interfaces. Novel experiments and molecular dynamics (MD) simulations allow oil flow and oil-CO_2 exchange to be quantified in analog and real nanopores. The study will ultimately illustrate how nanopore-flow phenomena affect oil-CO_2 transport in shale and tight oil reservoirs and provide insight for proper upscaling from nanoscale understanding to reservoir scale simulations. We experimentally investigated CO_2 adsorption in nanopores using anodic aluminum membranes (AAO). Flow rates of oil represented by hexane (C_6), decane (C_{10}), and hexadecane (C_{16}) were measured in the experiments under a constant pressure gradient and the permeability improvements due to interfacial CO_2 estimated. The experimental results were used to validate and calibrate MD-simulations that were performed to investigate the modulating effect of interfacial CO_2 on C_{10} and C_{16} flow in nanopores. Findings of the experiments and MD simulations indicate that flow modulation due to adsorbed CO_2 is accentuated in heavier oils. On the other hand, a negative effect of interfacial CO_2 on C_6 permeability was observed in the experiments. These results emphasize the significance of the reservoir oil composition in the design and operation of huff-n-puff projects. The findings can ultimately contribute to the optimization of CO_2 EOR operational parameters such as injection pressure and soak time to maximize oil recovery and stored CO_2.

Introduction

Unconventional oil and gas reservoirs have transformed the US oil industry, with shale formations like Bakken, Eagle Ford, and Permian Basin driving US unconventional production from 16.5% in 2008 to approximately 60% by 2019 (EIA 2019). Despite this growth, recovery factors remain low; for example, in the Bakken field, the recovery factor is estimated to be less than 8% (Jin et al. 2017; Sheng 2015). CO_2

huff-n-puff injection presents an opportunity to enhance oil recovery while enabling carbon storage. In unconventional reservoirs, however, this method faces some challenges, including limited matrix injectivity and gas bypassing (Wang et al. 2017). While field tests demonstrate improved production performance (Sheng 2017; Louk et al. 2017; Ellafi and Jabbari 2020), knowledge gaps regarding optimal operational parameters persist (Todd and Evans 2016). Advancing this technology requires improved understanding of oil and CO_2 flow dynamics at both nanopore and reservoir scales.

Reservoir simulation is an important tool for predicting production and planning operations in unconventional reservoirs. However, commercial simulators that are mostly based on conventional reservoir flow physics (Yu et al. 2015) are inadequate for unconventional reservoirs where nanofluidic physics influences flow behavior. In nanopores, which dominate unconventional reservoirs, confinement and interfacial forces can affect oil-CO_2 transport (Karniadakis et al. 2006). These interfacial effects can be significant even when viscous flow is dominant. Research by Freund (2002) and Chen et al. (2008) has shown that confinement by pore walls and fluid surface forces lead to unconventional fluid behaviors such as interfacial fluid thickening and surface slippage effects (Barrat and Bocquet 1999; Joly et al. 2004). In CO_2 huff-n-puff operations these effects become more significant at later stages of the "puff" or soaking periods when injection pressure dissipates in narrow dead-end pores in the reservoir. Viscous flow is dominant in fractures at earlier stages of the cycles before injection pressure dissipates.

To quantify the modulation of oil flow by interfacial CO_2, Moh et al. (2020) performed MD simulations. Simulation results showed that CO_2 modulated hydrocarbon flow by adsorbing on calcite walls by replacing and displacing the adsorbed C_{10}. The resulting permeability changes were nonlinear: The pore permeability decreased at low CO_2 adsorption densities and then increased at moderate to high density levels. This enhancement effect is more pronounced in smaller pores, reaching 20-30% in 8 nm pores compared to only 10% in 15-30 nm pores. Despite these computational insights, experimental quantification of flow enhancement by interfacial CO_2 and related nanofluidic phenomena, such as diffusioosmosis, remains limited and is worth further investigation.

Zhu et al. (2019) examined the sieving properties of Niobrara shale through experiments and MD simulations using hydrocarbon mixtures. Their research revealed that during the flow of a C_{10} and C_{17} mixture through a Niobrara core sample, heavier hydrocarbons (C_{17}) were selectively hindered with downstream fluid showing higher concentration of C_{10} and lower concentration of C_{17} compared to the upstream injected fluid. MD simulations confirmed that this selective hindrance resulted not only from molecular size differences but also from stronger adsorption tendencies of C_{17} on calcite pore walls. Additional research has identified similar hindrance effects due to reduced diffusivities of hydrocarbon components in crowded media and anomalous diffusion combined with adsorption (Coskuner et al. 2021; Yildirim and Ozkan 2023).

To expand the findings of Zhu et al. (2019) and Coskuner et al. (2021) to study CO_2's role in huff-n-puff operations, the core samples previously injected with oil (C_{10} and C_{17} mixture) were soaked with CO_2 for 10 days at 600 psi, then the hydrocarbon mixture of the same composition was pumped through the samples again (Zhu et al. 2020a). The results of these experiments showed a decrease in the C_{10} composition and an increase in the C_{17} composition of the effluent fluid when production was restarted after the soaking period. However, this effect was transient and the C_{10} and C_{17} compositions returned to the level before soaking, which is the basis of the huff-n-puff method. The experimental results were verified by the MD simulations. It was shown that, before CO_2 injection, C_{17} molecules were adsorbed on the pore walls due to their higher adsorption tendency than C_{10} molecules. However, because of the preferential adsorption of CO_2 on the calcite pore walls, C_{17} molecules were stripped from the pore surface and mixed with the bulk (free phase) hydrocarbon mixture. When all adsorption sites were occupied by CO_2 molecules, further injection of CO_2 created the well-known oil swelling effect and eventually, helped displacement of the fluid mixture through the system.

Similar experiments and MD simulations using Niobrara crude oil showed comparable results where before CO_2 injection, the composition of lighter components (C_3-C_6) increased while the composition of heavier components (C_{11}-C_{20}, C_{20}+) decreased in downstream fluid (Zhu et al. 2020b). After CO_2 soaking, a compositional shift occurred due to the release of previously hindered heavy components, causing increases in C_7-C_{10}, C_{11}-C_{20}, and C_{20}+ fractions above their initial concentrations. MD simulations from Zhu et al. (2020b) again showed that these observations were due to CO_2 adsorbing on the calcite pore, stripping heavier hydrocarbon components previously adsorbed on the pore surface and increasing the heavier components in the free oil phase, and swelling the heavier hydrocarbon mixture to increase its mobility. While these experiments and simulations demonstrated the adsorption tendencies of hydrocarbon components and the role that interfacial CO_2 plays to enhance their recovery, the flow enhancement was not quantified experimentally due to the heterogeneity of the pore structure in Niobrara core samples. To that end, Zhu (2020) attempted to analyze adsorbed and free phase compositions in crushed Niobrara samples immersed in oil using gas chromatography. This method proved challenging due to hydrocarbon vaporization and composition changes too subtle for detection via standard gas chromatography techniques.

Our previous publication (Hegazy et al. 2024) introduced an experimental setup to quantify permeability enhancement in nanopores due to interfacial CO_2. Instead of using shale rock samples, anodic aluminum oxide (AAO) membranes were used because of their uniform pore size (10 nm), fixed pore density and uniform pore structure, which helped estimating permeability with less uncertainty due to heterogeneity. Experimental results showed a pore-permeability increase of 15% due to interfacial CO_2. The results supported the finding from MD simulations of Moh et al. (2020).

This paper presents additional new findings of the MD simulations and experiments, which verify the previous results and help to quantify oil-flow modulation in nanopores due to interfacial CO_2. This phase of the study utilizes the same experimental setup described by Hegazy et al. (2024) to measure permeability improvement to lighter (C_6) and heavier (C_{16}) hydrocarbons due to adsorbed CO_2. Furthermore, MD simulations using C_{16} were performed and validated by experimental results. The experiments previously reported (Hegazy et al. 2024) have also been rerun by using CO_2 dissolved in C_{10} to ensure repeatability and mitigate instability in initial rate readings. The ultimate objective of this study is to improve understanding of nanofluidic physics to be used in reservoir-scale numerical simulators and provide data to simulate the CO_2 huff-n-puff performance in unconventional reservoirs.

Experimental and Simulation Methodology

To measure permeability enhancement due to interfacial CO_2, initial experiments determined baseline permeability using only oil (C_6, C_{10} and C_{16}). The experiment maintained constant differential pressure by pumping deionized water with an upstream Teledyne pump into a transfer vessel, pushing oil through an Anodic Aluminum Oxide (AAO) membrane in a membrane holder. Flow rates were recorded as oil passed through the membrane into a downstream transfer vessel connected to a lower pressure receiving pump, as shown in Figure 1. With known oil viscosities at experimental conditions (NIST Chemistry Webbook 2023), permeability was calculated using Darcy's (1856) equation with the measured differential pressure and flow rates. The experimental setup and conditions are explained in further detail in Hegazy et al. (2024). Experimental pressures, temperatures and viscosities are presented in Table 1.

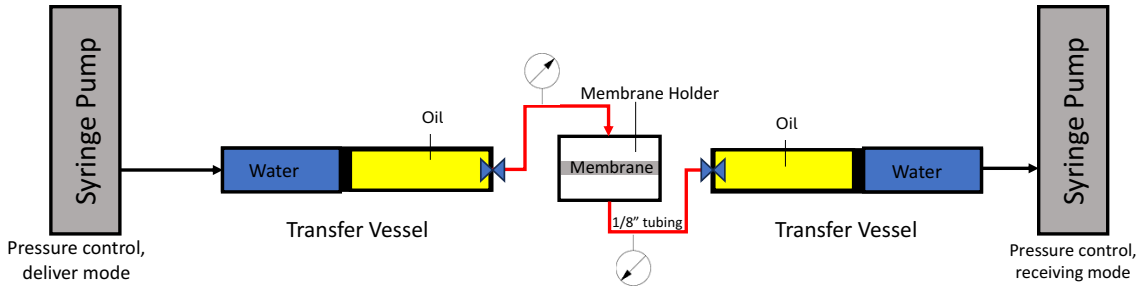

Figure 1. Schematic diagram of experimental setup for oil (C6, C10 or C16) only permeability measurements

Table 1. Experiment pressure and temperature settings and fluid viscosities of oil

Oil	Inlet Pressure (psi)	Outlet Pressure (psi)	Net Pressure (psi)	Ambient Temperature (F)	Viscosity (cp)
C_6	422	400	22	72	0.317
C_{10}	400	200	200	72	0.93
C_{16}	430	400	30	72	3.415

A slight alteration in the setup was required for the second set of experiments that measure membrane permeability to oil with dissolved CO_2. A T-connection was added to the upstream transfer vessel and connected to equalize the pressure between the inlet and the outlet of the membrane holder at ~ 400 psi to prevent membrane breakage. The gradual increase in pressure from 0 psi to reach experimental pressure would result in an initial two-phase oil and CO_2 mixture, which could result in CO_2 not properly dissolving in the oil and instable flow during the experiment (Figure 2). The setup is discussed in more detail in Hegazy et al. (2024). The oil and CO_2 were mixed at immiscible conditions since the membrane holder cannot withstand pressures exceeding 450 psi. A PVT simulator was used to calculate the hydrocarbon and CO_2 composition so that the mixture is at single liquid phase under experimental pressure and temperature conditions. A summary of the compositions of the studied mixtures (C_6+ CO_2, C_{10}+ CO_2, C_{16}+ CO_2), pressure and temperature settings and mixture viscosities is presented in Table 2. Lower differential pressure is required between the inlet and the outlet to maintain single, liquid-phase fluid in the inlet and outlet of the membrane holder.

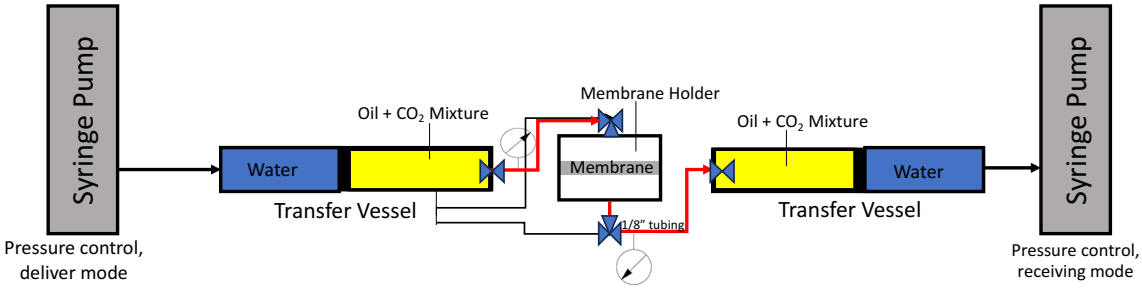

Figure 2. Schematic diagram of updated experimental setup for oil (C_6, C_{10} or C_{16}) and CO2 mixtures

Table 2. Composition, viscosity and pressure/temperature of Oil and CO_2 mixtures used in the second set of experiments

Fluid	Component	Mole (%)	Inlet Pressure (psi)	Outlet Pressure (psi)	Net Pressure Drop (psi)	Viscosity (cp)	Temperature (F)
C_6+CO_2	C_6	67	420	380	40	0.317	73
	CO_2	33					
C_{10}+CO_2	C_{10}	83	420	385	35	0.855	73
	CO_2	17					
C_{16}+CO_2	C_{16}	93.2	430	400	30	3.06	73
	CO_2	6.8					

To help understand permeability modulation by interfacial CO_2, molecular dynamics (MD) simulations were performed. MD simulations explicitly demonstrate the distribution and transport of interfacial oil and CO_2 molecules and thus are a good tool to elucidate the mechanisms underlying permeability modulation. MD simulation of fluid transport through the 10 nm-diameter nanopores used experimentally is expensive because of the large number of molecules that must be included in round pores. However, previous studies (Qiao and Aluru 2003; Karniadakis et al. 2006; Wu et al. 2017) have shown that in such wide pores, fluid flow can be predicted accurately by the classical flow theories when flow characteristics near the fluid-wall interface (in particular, the slippage behavior) are accurately parameterized into theories. Since the interfacial zone's width (typically, a few fluid atom diameters) is much smaller than 10 nm, its flow characteristics can be studied using pores with the same material but no curvature, i.e., slit-shaped Al_2O_3 nanopores.

We designed two MD systems to study the interfacial transport of pure C_{16} and C_{16}+CO_2 mixtures. The first system consists of a slab of C_{16} enclosed between two Al_2O_3 walls (Figure 3a). The second system has a similar setup except that C_{16} is replaced with a C_{16}+CO_2 mixture (Figure 3b). Each Al_2O_3 wall measures 5.77 nm × 3.33 nm in the lateral (*x*-*y*) plane and 2.46 nm in the normal (*z*) direction, respectively. The pore width in both systems were 9.58 nm, which is wide enough to ensure that fluids at the pore center behave as bulk-phase. The number of C_{16} molecules in the first system was tuned so that the pore pressure, as determined by summing the forces acting on the upper wall, is 430 psi; same as the inlet pressure adopted in our experiments (see Table 1). The number of C_{16} and CO_2 molecules in the second system is tuned to maintain this pressure and the mole fraction of CO_2 in the pore center, where the C_{16}+CO_2 mixture is bulk-like, reached 6.9% as in the experiment.

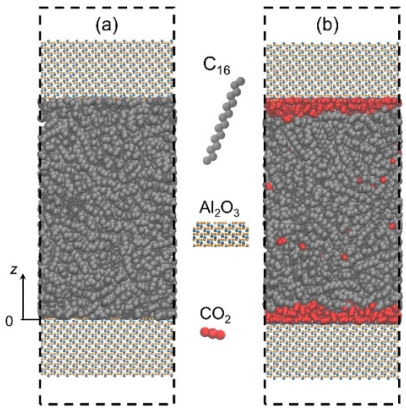

Figure 3. Snapshots of MD simulation systems for studying transport of C_{16}-CO_2 mixture (a) and pure C_{16} (b) in aluminum oxide nanopores. The dashed lines denote the periodic simulation box.

Each Al_2O_3 wall was cut from an Al_2O_3 crystal in the (001) plane and described by the INTERFACE force fields (Jo et al. 2008; Choi et al. 2021). The force fields for CO_2 and C_{16} were taken from (Zhu et al. 2009) and the NERD force field (Nath et al. 1998), respectively. Moreover, the cross interactions between CO_2 and C_{16} followed the method in Wang et al. (2018), which was shown to predict the phase diagram of hydrocarbon-CO_2 mixture well.

MD simulations were performed using the LAMMPS package (Plimpton 1995) in the NVT ensemble. The temperature was kept at 295 K. After the pore pressure was adjusted to the target value using the approach described above, each system was equilibrated for 10 ns. This followed by a production run during which an acceleration of 0.0015 nm/ps^2 was applied to fluid atoms in the *x*-direction to drive fluid transport. The production run lasted 80 ns, with results during the last 70 ns used for analysis. In the flow simulation, the thermostat was applied only to the *y* and *z* components of the fluid's velocity to avoid biasing the fluid flow. A cutoff of 1.2 nm was used for computing Lennard-Jones potentials, and the electrostatic interactions were calculated using the PPPM solver (Eastwood et al. 1980).

Results

Experimental results indicate that during CO_2-EOR operations, such as huff and puff, CO_2 modulates oil flow not only by viscosity reduction, but also by adsorbing into the nanopore wall and displacing hydrocarbon molecules into the bulk phase. This section presents the experimental rates through the AAO membrane and calculated permeability improvements to C_6, C_{10} and C_{16} due to interfacial CO_2.

In Hegazy et al. (2024), pore permeability to C_{10} and C_{10} with dissolved CO_2 were measured. Figure 4 shows the recorded rate of C_{10} at a differential pressure of 200 psi. Based on the viscosity in Table 1 and stabilized recorded rate (0.15 cc/min - 0.2 cc/min) divided by the pore density in the membrane, single pore permeability was calculated to be 0.0064 mD. Further detail on the permeability calculation is presented in Hegazy et al. (2024). Based on Poiseuille's law, at 10 mn pore diameter pore permeability is 0.003 mD. The higher measured permeability could be a consequence of slippage (Barrat and Bocquet 1999) and shear effects (Metin et al. 2013) that can result from complexities of nanoscale flow and confinement in pores due to high pressure.

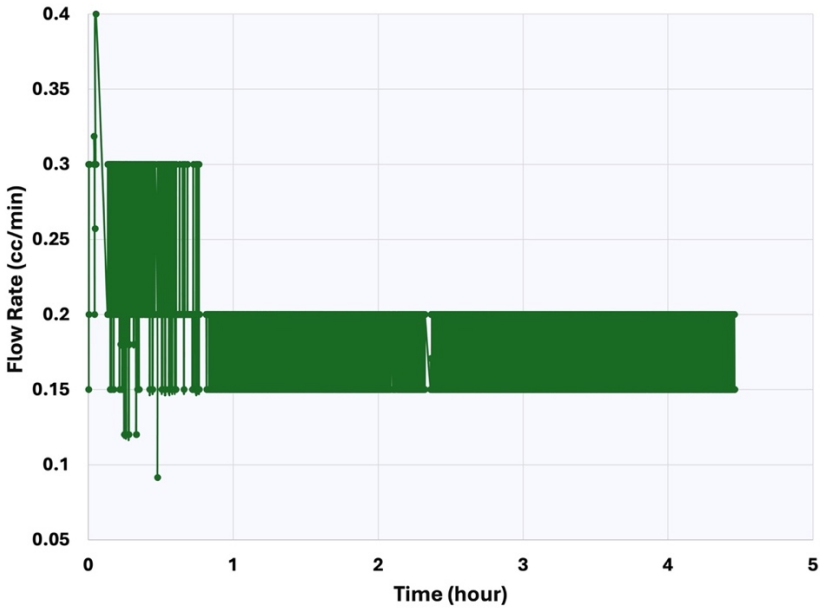

Figure 4. Decane(C_{10}) flow rate through the AAO membrane vs time

The experiment to measure pore permeability to C_{10} + CO_2 reported in Hegazy et al. (2024) was repeated to minimize the early-time instabilities suspected to be caused by insufficient mixing of the two components. Like in Hegazy et al. (2024), lower rates were observed during the first few hours of the experiment followed by a relatively stabilized rate (fluctuating between 0.032 cc/min and 0.046 cc/min) (Figure 5). Unstable fluctuations that were shown in Hegazy et al. (2024) were reduced by also prefilling tubing connected to the membrane with oil to minimize the entrapped air in the system and by shaking the transfer vessel throughout the experiment duration.

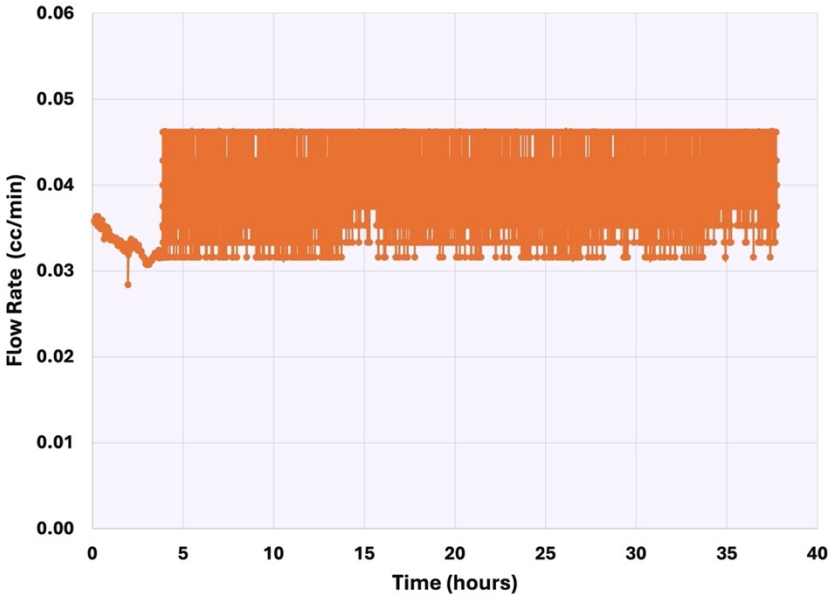

Figure 5. Decane(C_{10}) with dissolved CO_2 flow rate through the AAO membrane vs time

Pore permeabilities to C_{10} ($k_{c_{10}}$) only and C_{10} + CO_2 ($k_{c_{10}+CO_2}$) from experimental results were computed using the pumped fluid viscosities of 0.93 cp and 0.855 cp respectively. Therefore, enhancement in permeability due to interfacial CO_2 is calculated as follows:

$$\text{Permeability increase due to interface } CO_2 = \frac{k_{c_{10}+CO_2} - k_{c_{10}}}{k_{c_{10}}} = \frac{0.007-0.006}{0.006} = 0.16. \quad \text{.....(1)}$$

The 16% permeability improvement due to interfacial CO_2 supports the conclusions from MD simulations performed by Moh et al. (2020) for 8 nm-15 nm diameter calcite pores at high CO_2 adsorption densities.

Flow behavior observed by C_{16} was very different from C_{10}. Experimental results show that C_{16} flow is clearly hindered, flowing at extremely low flow rates compared to C_{10}. Flow rates observed during the experiment were intermittent and fluctuating as shown in Figure 6. The plot shows that the flow rate fluctuates between 0.0015 cc/min and 0.0005 cc/min (Figure 6), so an average rate of 0.001 cc/min was used in the permeability calculation. By using the viscosity from Table 1 (3.415 cp) and the same membrane parameters used for C_{10} in Darcy's equation, permeability to a single pore to C_{16} is 0.00085 mD. This permeability is much lower than the measured permeability to C_{10}, indicating hindrance of the heavier hydrocarbon.

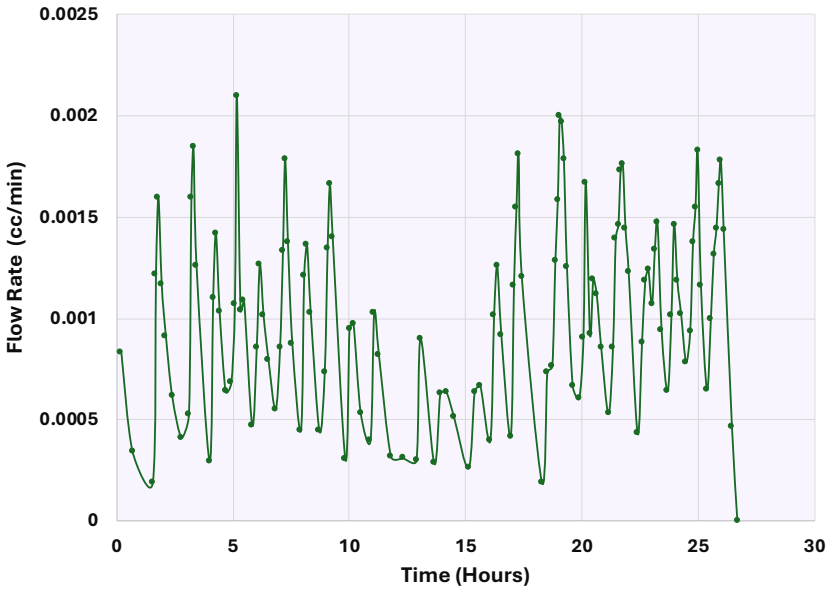

Figure 6. Hexadecane (C_{16}) flow rate through the AAO membrane vs time

Mixing C_{16} with CO_2 resulted in significant permeability enhancement. A plot of the flow rate of the mixture through the membrane vs. time is shown in Figure 7. Similar flow behavior as C_{16} only is observed where rate is fluctuating throughout the experiment. A median rate of 0.021 cc/min was used as input to the permeability calculation. The membrane permeability computed based on this rate combined with the net pressure and viscosity in Table 2 is 0.001575 mD. Based on the calculation method described in Eq. 1, permeability enhancement for C_{16} due to interfacial CO_2 is 84%. The comparison of C_{16} and C_{10} experimental results illustrates that interfacial CO_2 plays a greater role in modulating heavy hydrocarbons. This high increase in permeability enhancement compared to C_{10} experiments and results from the simulations by Moh et al. (2020) makes MD simulations to investigate how interfacial CO_2 modules C_{16} flow worthwhile. These simulations are discussed in the following sections of this paper.

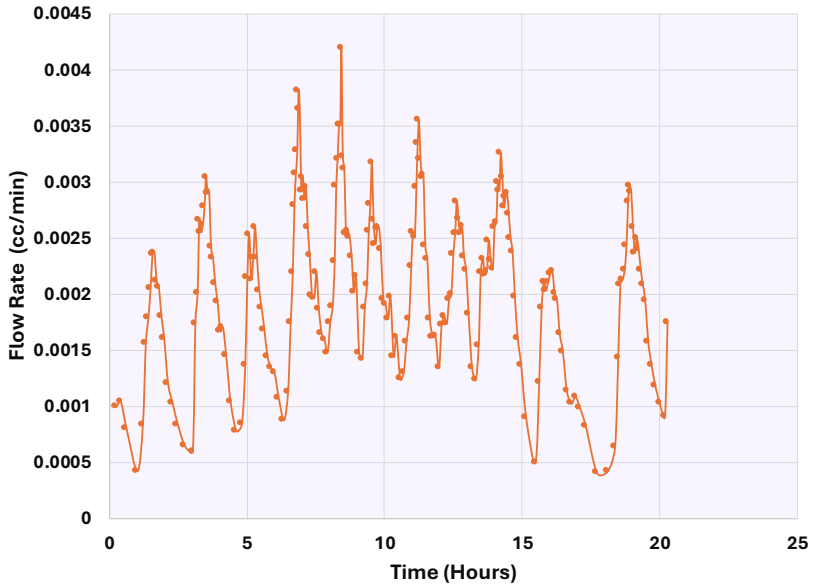

Figure 7. Hexadecane (C_{16}) with dissolved CO_2 flow rate through the AAO membrane vs time

The effect of CO_2 on the flow of the lighter hydrocarbon (C_6) was also experimentally investigated. The experimental results align with the findings from Zhu et al. (2020) where the composition of C_3-C_6 decreases following CO_2 soaking. Figure 8 shows the flow rate of C_6 vs. time. At a differential pressure of 22 psi, the rate fluctuates mostly between 0.055 cc/min and 0.075 cc/min through the experiment. Using the average measured rate of 0.065 cc/min and input from Table 1, permeability to C_6 is 0.007 mD.

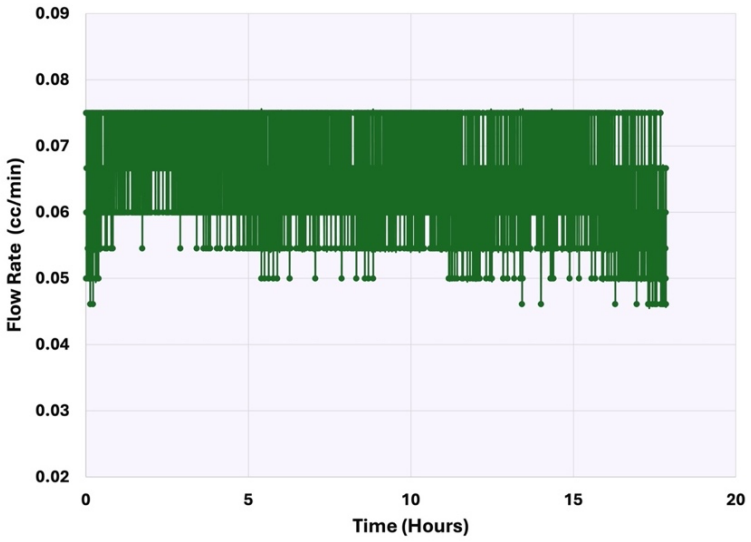

Figure 8. Hexane (C_6) flow rate through the AAO membrane vs time

Dissolving CO_2 in C_6 resulted in a lower measured permeability. Figure 9 shows the recorded flow rate at a net pressure of 40 psi, showing an initial low rate of 0.01 cc/min that rises to a relatively stabilized rate that fluctuated between 0.04 and 0.055 cc/min. The median rate within the stabilized flow period at a 40 psi net pressure and a viscosity of 0.317 cp yields a permeability of 0.003 mD. Following Eq. 1, this means a 60% decrease in permeability due to interfacial CO_2. These results require further experimental analysis before MD simulations could be performed.

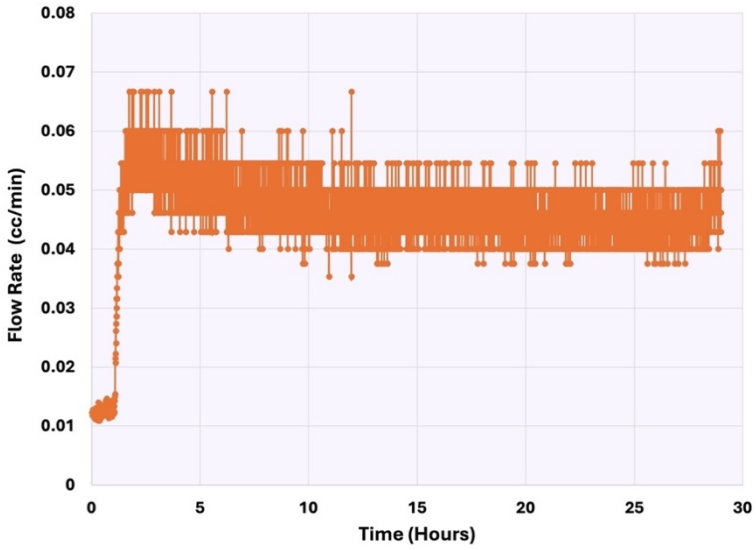

Figure 9. Hexane (C_6) with dissolved CO_2 flow rate through the AAO membrane vs time

To help understand the modulation of C_{16} transport by CO_2, for which the experimental data are robust, we now analyze the MD results obtained for transport of pure C_{16} and C_{16}+CO_2 mixtures. Figure 10a and Figure 10b show the density profiles of C_{16} and CO_2 in the two systems. For the pure C_{16} system, C_{16} adsorb on the pore walls distinctly, as evident from the sharp density peak at around z = 0.2 nm. This adsorption is driven by van der Waals forces because C_{16} is highly nonpolar. In the C_{16}+CO_2 mixture, although the bulk mole fraction of CO_2 is only 6.9%, copious adsorption of CO_2 in the form of two adsorption layers corresponding to the two density peaks in Figure 10b is evident. CO_2 molecules completely displace the C_{16} molecules from the pore walls. These results align well with the strong adsorption of CO_2 on various inorganic pore walls reported recently (Peng et al. 2020; Zhang et al. 2021; Zhang et al. 2022; Zhang et al. 2024). The more preferred adsorption of CO_2 on the Al_2O_3 pore walls with a strong ionic nature originates from the charge-quadrupole interactions between the CO_2 molecules and the wall atoms, which are much stronger than the van der Waals interactions between C_{16} and pore walls.

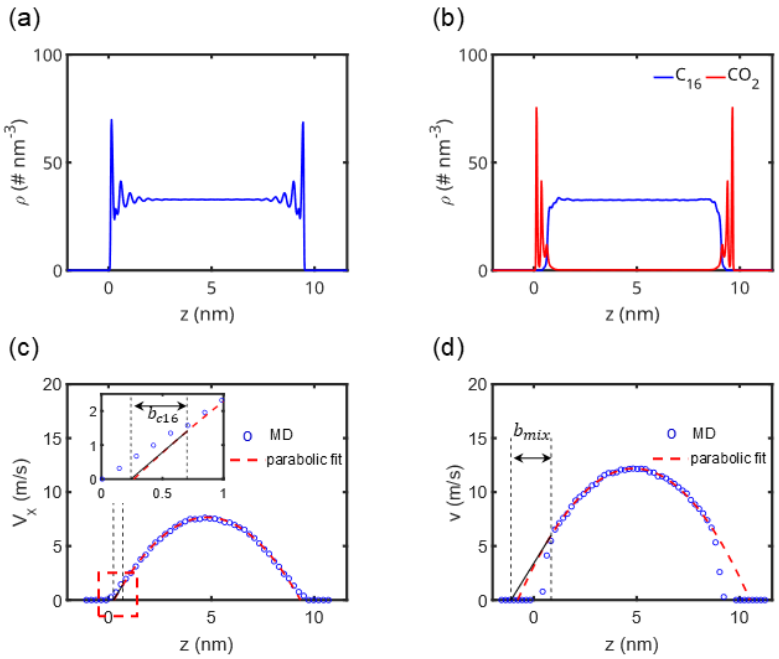

Figure 10. (a, b) Density profiles of the carbon atoms in pure C_{16} (a) and C_{16}+CO_2 mixture (b) across the nanopore. (c, d) Velocity profiles of C_{16} across nanopore filled with pure C_{16} (c) and C_{16}+CO_2 mixture (d).

Figure 10c and Figure 10d show the velocity profiles of C_{16} in the two systems. In both systems, the velocity profile in the central portion of the pore can be fitted well to a parabolic profile, as expected for flow in wide nanopores. In the pure C_{16} system, a slip is observed. The slip length b at the wall-fluid interface can be extracted using $V_s = b(\partial V_x/\partial z)|_{z=z_w}$, where V_s is the slip velocity measured at the effective position of the wall ($z = z_w$). Using the velocity profile in Figure 10c, a small slip length of $b_{c16} = 0.45 \pm 0.08$ nm was obtained. In the C_{16}+CO_2 mixture system, a larger slip length of $b_{mix} = 1.90 \pm 0.26$ nm was obtained. The larger slip length in the C_{16}+CO_2 mixture system is caused by the fact that, small and mobile molecules in the CO_2 adsorption layer serve as an effective lubricant for the bulky C_{16} molecules next to them, which is in sharp contrast to the pure C_{16} case, where C_{16} molecules adsorbed on pore walls cannot easily slide over the immobile, rigid pore walls. The stronger slippage in the mixture system leads to the stronger flow in it.

The above results show that the oil flow in wide nanopores can be described well using classical theories except that a finite slip length should be considered. Therefore, we can compute the permeability of the round nanopores in our experiments through:

$$K = \frac{a^2}{8}\left(1 + \frac{4b}{a}\right). \quad \ldots\ldots\ldots\ldots\ldots\ldots\ldots\ldots (2)$$

where a is the pore radius (5 nm) and b is the slip length. The ratio of the mobility of pores with pure C16 and C_{16}+CO_2 mixture, β, is

$$\beta = \frac{K_{mix}}{K_{c16}} = \frac{1 + \frac{4b_{mix}}{a}}{1 + \frac{4b_{pure}}{a}}. \quad \ldots\ldots\ldots\ldots\ldots\ldots\ldots\ldots (3)$$

Substituting the slip lengths obtained above and using a radius of 5 nm, we obtain $\beta = 1.86 \pm 0.17$. The computed β is in remarkable agreement with the value of 1.84 measured experimentally.

Discussion

The experiments provide an insight on flow behavior of individual hydrocarbon components. A notable observation is that C_{16} flow rate was extremely low compared to C_6 and C_{10}, indicating that it was hindered. These results align with findings from Zhu et al. (2020) which state that the hindrance could not only be attributed to the chain length and high viscosity, but also the higher tendency of the heavier hydrocarbon components to adsorb on pore walls. Another observation is that flow rate of C_6, C_{10} and C_{16} was fluctuating throughout their respective experiments with C_{16} flowrate fluctuating drastically, which could be due to the complexity of the experimental setup and transfer vessel piston behavior. The intense piston behavior observed by C_{16} could be explained by Mustafa et al. (2020) who showed that hexadecane (C_{16}) molecules in nanopores can demonstrate piston-like behavior because when they pass through pores, their long chain can go through conformational changes. The conformational changes along with the higher adsorption tendencies (Zhu et al. 2020) exhibited by C_{16} can cause high flow rate fluctuations compared to the lighter hydrocarbon components (C_6 and C_{10}). Also, trapped air might contribute to flow instabilities during the experiment.

Permeability enhancement due to interfacial CO_2 varied greatly between the tested hydrocarbon components. In $C_{10,}$ as previously highlighted by Hegazy et al. (2024), permeability improvement due to interfacial CO_2 is close to the results from MD simulations performed by Moh et al (2020). Experiments investigating the lighter hydrocarbon (C_6) showed a 60% decrease in permeability after mixing the oil with CO_2. Although these findings align with findings from Zhu et al. (2020), these researchers observed only a 15% decrease in mol %. The significant decline in permeability observed in this study could be due to the higher molar composition of CO_2 (33%). Since C_6 has low affinity to adsorb on the pore wall (Zhu et al. 2020), when CO_2 adsorbs on the pore wall it reduces effective pore diameter causing a reduction in permeability. Furthermore, as CO_2 adsorbs onto the pore wall, given the hypothesis by Zhu et al. (2020), it may not displace a notable volume of C_6 that would contribute to the permeability increase due to interfacial CO_2. It can also be hypothesized that viscous forces are also not playing a role in modulating flow since viscosity of the fluid does not change as a result of mixing CO_2 with C_6. These results need to be investigated further to assess the impact of CO_2 concentration on C_6 permeability, first experimentally and followed by MD simulations. Contrary to the results of C_6 experiments, results from the C_{16}+CO_2 experiments showed a significant increase of permeability (84%) to C_{16} due to interfacial CO_2. Such a permeability enhancement is predicted quantitatively by the classical permeability model parameterized using the slip length extracted from MD simulations. While the excellent agreement between experiment and simulation is perhaps fortuitous, it is safe to conclude that CO_2 adsorption-induced slippage contributes greatly to the experimentally observed permeability enhancement.

The results presented in this paper illustrate the potential impact of nanofluidic physics on outcomes of CO_2 huff-n-puff operations. There are indeed other phenomena that are worth investigating such as diffusioosmosis. Nanofluidic physics can be incorporated into reservoir scale simulators to assess how its effect can impact oil recovery and carbon storage in CO_2 huff-n-puff field cases.

Conclusions

Experiments utilizing synthetic AAO membranes were performed to quantify the permeability enhancement to C_6, C_{10} and C_{16} due to interfacial CO_2, while isolating the effect of viscosity reduction. The first set of experiments computed permeability of the membrane to oil only (C_6, C_{10} and C_{16}) before experiments to measure flowrate of oil with dissolved CO_2. Experiments indicated that flow of the heaviest component C_{16} was clearly hindered. The second set of experimental results indicated that permeability to C_6 decreased because of mixing it with CO_2. However, the experiments showed that interfacial CO_2 mitigated the hindrance and resulted in significant enhancement of pore permeability to C_{16}. MD simulations results show that such an enhancement is attributed to the stronger slippage of C_{16} near the pore walls, which is in turn caused by the effective lubrication of C_{16} flow by the adsorbed CO_2 molecules. These results point out the importance of considering nanofluidic phenomena in reservoir simulations for CO_2 EOR projects in unconventional reservoirs.

Acknowledgment

This material is based upon work supported by the NSF Award Number 2246274, GOALI: "Nanofluidics of CO_2 Utilization and Storage in Tight Oil Reservoirs." Any opinions, findings, and conclusions or recommendations expressed in this material are those of the author(s) and do not necessarily reflect the views of the National Science Foundation. Portions of this material will appear in the PhD dissertation of Dina Hegazy at Colorado School of Mines.

References

Aimei, Z., Zhang, X., Qinglin, L., et al. 2009. A Fully Flexible Potential Model for Carbon Dioxide. *Chinese Journal of Chemical Engineering* **17**(2): 268-272. https://doi.org/10.1016/S1004-9541(08)60204-9.

Barrat, J. L., and Bocquet, L. 1999. Large Slip Effect at a Nonwetting Fluid-Solid Interface. *Phys. Rev. Lett*. **82** (23): 4671-4674. doi: https://doi.org/10.1103/PhysRevLett.82.4671.

Chen, Y. F., Ni, Z. H., Wang, G. M., Xu, D. Y., and Li, D. Y. 2008. Electroosmotic Flow in Nanotubes with High Surface Charge Densities. *Nano Letters* **8** (1): 42-48. http://doi.org/10.1021/nl0718566.

Choi, Y. K., Park, S.-J., Park, S., et al. 2021. CHARMM-GUI Polymer Builder for Modeling and Simulation of Synthetic Polymers. *Journal of Chemical Theory and Computation* **17**(4): 2431-2443. https://doi.org/10.1021/acs.jctc.1c00169.

Coskuner, Y., Yin, X., and Ozkan, E. 2021. Effects of Molecular Level Forces on the Diffusivity Characteristics of Hydrocarbons in Shale Reservoirs. Paper presented at the SPE/AAPG/SEG Unconventional Resources Technology Conference, Houston, Texas, USA, 26-28 July. URTEC-2021-5680-MS. https://doi.org/10.15530/urtec-2021-5680.

Darcy, H. 1856. The Public Fountains of the City of Dijon: Exposition and Application of Principles to Follow and Formulas to Use in Questions of Water Distribution. Paper presented at Victor Dalmont, Paris.

Eastwood, J. W., Hockney, R. W. and Lawrence, D. 1980. P3M3DP-The three-dimensional periodic particle-particle/particle-mesh program. *Computer Physics Communications* **19**(2): 215-261.

EIA. 2019. Annual Energy Outlook 2019 with Projections to 2050. U.S. Energy Information Administration, Washington, DC (March 2019).

Ellafi, A. and Jabbari, H. 2020. Understanding the Mechanisms of Huff-n-Puff, CO_2-EOR in Liquid-Rich Shale Plays: Bakken Case Study. Presented at the SPE Canada Unconventional Resources Conference, 28-30 September. SPE-200001-MS. http://dx.doi.org/10.2118/200001-MS.

Fang, C., Yin, X. and Qiao, R. 2020. Interfacial CO_2-mediated nanoscale oil transport: from impediment to enhancement. *Physical Chemistry Chemical Physics* **22**(40): 23057-23063. https://doi.org/10.1039/D0CP03930F.

Freund, J. B. 2002. Electro-osmosis in a nanometer-scale channel studied by atomistic simulation. *Journal of Chemical Physics* **116** (5): 2194-2200. https://doi.org/10.1063/1.1431543.

Hegazy, D. A., Yin, X., Qiao, R., and Ozkan, E. 2024. Experimental Study to Investigate CO_2 Mediated Oil Flow in Nanopores. Paper presented at the SPE Annual Technical Conference and Exhibition, New Orleans, Louisiana, USA, 23–25 September. SPE-220726-MS. https://doi.org/10.2118/220726-MS

Hoffman, B. T. and Evans, J. G. 2016. Improved Oil Recovery IOR Pilot Projects in the Bakken Formation. Presented at the SPE Low Perm Symposium, Denver, Colorado, 5-6 May. SPE-180270-MS. http://dx.doi.org/10.2118/180270-MS.

Jin, L., Sorensen, J. A., Hawthorne, S. B., Smith, S. A., Pekot, L. J., Bosshart, N. W., Burton-Kelly, M. E., Miller, D. J., Grabanski, C. B., Gorecki, C. D., Steadman, E. N., and Harju, J. A. 2017. Improving Oil Recovery by Use of Carbon Dioxide in the Bakken Unconventional System: A Laboratory Investigation. *SPE Res Eval & Eng* **20** (3): 602–612. SPE-178948-PA. http://dx.doi.org/10.2118/178948-PA.

Joly, L., Ybert, C., Trizac, E., and Bocquet, L. 2004. Hydrodynamics within the Electric Double Layer on Slipping Surfaces. *Phys. Rev. Lett*. **93** (25), 257805. doi: https://doi.org/10.1103/PhysRevLett.93.257805.

Jo, S., Kim, T., Iyer, V. G., et al. 2008. CHARMM-GUI: a Web-based Graphical User Interface for CHARMM. *Journal of Computational Chemistry* **29**(11): 1859-1865. https://doi.org/10.1002/jcc.20945.

Karniadakis, G., Beskok, A. and Aluru, N. 2006. *Microflows and Nanoflows: Fundamentals and Simulation*, Springer Science & Business Media.

Louk, K., Ripepi, N., Luxbacher, K., Gilliland, E., Tang, X., Keles, C., Schlosser, C., Diminick, E., Keim, S., Amante, J., and Michael, K. 2017. Monitoring CO_2 Storage and Enhanced Gas Recovery in Unconventional Shale Reservoirs: Results from the Morgan County, Tennessee Injection Test. *J. Nat. Gas Sci. Eng* **45**: 11-25. http://dx.doi.org/10.1016/j.jngse.2017.05.024.

Metin, C., Bonnecaze, R. T., and Nguyen, Q. P. 2013. The Viscosity of Silica Nanoparticle Dispersions in Permeable Media. SPE Res Eval & Eng 16 (3): 327–332. SPE-157056-PA. https://doi.org/10.2118/157056-PA.

Moh, D., Fang, C., Yin, X., and Qiao, R. 2020. Interfacial CO_2-Mediated Nanoscale Oil Transport: From Impediment to Enhancement. Physical Chemistry Chemical Physics 22 (40): 23057-23063. https://doi.org/10.1039/D0CP03930F

Moh, D. Y., Zhang, H., Sun, S., et al. 2022. Molecular anatomy and macroscopic behavior of oil extraction from nanopores by CO_2 and CH_4. *Fuel* **324:** 124662. https://doi.org/10.1016/j.fuel.2022.124662.

Mustafa, S.F.Z., Maarof, H., Ahmed, R., and Abdallah, H.H. 2020. Diffusional and Conformational Behaviour of Hexadecane-1,16-Diol and Hexadecane Enclathration in Three-Dimensional Nanoporous Urea Inclusion Compound Model Systems via Molecular Dynamics Simulation. *Computational Materials Science* **171**: 109198. https://doi.org/10.1016/j.compmatsi.2019.109198

Nath, S. K., Escobedo, F. A. and de Pablo, J. J. 1998. On the Simulation of Vapor–liquid Equilibria for Alkanes. *The Journal of Chemical Physics* **108**(23): 9905-9911. https://doi.org/10.1063/1.476429.

NIST Chemistry WebBook. 2023. NIST Standard Reference Database Number 69, https://webbook.nist.gov/chemistry/#Search (accessed 10 October 2024).

Peng, F., Xiong, K., Wang, R., et al. 2020. Molecular Insight into Microbehaviors of n-Decane and CO_2 in Mineral Nanopores. *Energy & Fuels* **34**(3): 2925-2935. https://pubs.acs.org/doi/10.1021/acs.energyfuels.9b04125.

Plimpton, S. 1995. Fast Parallel Algorithms for Short-range molecular dynamics. *Journal of Computational Physics* **117**(1): 1-19. https://doi.org/10.1006/jcph.1995.1039.

Qiao, R. and Aluru, N. R. 2003. Ion Concentrations and Velocity Profiles in Nanochannel Electroosmotic Flows. *The Journal of Chemical Physics* **118**(10): 4692-4701. https://doi.org/10.1063/1.1543140.

Sheng, J. J. 2015. Enhanced Oil Recovery in Shale Reservoirs by Gas Injection. *J. Nat. Gas Sci. Eng* **22**: 252–259. http://dx.doi.org/10.1016/j.jngse.2014.12.002.

Sheng, J. J. 2017. Critical Review of Field EOR Projects in Shale and Tight Reservoirs. *J. Pet. Sci. Eng* **159**: 654-665. http://dx.doi.org/10.1016/j.petrol.2017.09.049.

Wang, L., Tian, Y., Yu, X., Wang, C., Yao, B., Wang, S., Winterfeld, P. H., Wang, X., Yang, Z., Wang, Y., Cui, J., and Wu, Y.-S. 2017. Advances in Improved/Enhanced Oil Recovery Technologies for Tight and Shale Reservoirs. *Fuel* **210**: 425-445. http://dx.doi.org/10.1016/j.fuel.2017.08.095.

Wang, R., Peng, F., Song, K., et al. 2018. Molecular Dynamics Study of Interfacial Properties in CO_2 Enhanced Oil Recovery. *Fluid Phase Equilibria* **467:** 25-32. https://doi.org/10.1016/j.fluid.2018.03.022.

Wu, K., Chen, Z., Li, J., et al. 2017. Wettability Effect on Nanoconfined Water Flow. *Proceedings of the National Academy of Sciences* **114**(13): 3358-3363. https://doi.org/10.1073/pnas.1612608114.

Yildirim, G., and Ozkan, E. 2023. Effect of Gas-Liquid Anomalous Diffusion on Production Behavior and Pressure and Rate Transient Responses in Unconventional Reservoirs. Paper presented at the SPE/AAPG/SEG Unconventional Resources Technology Conference, Denver, Colorado, USA, 13–15 June. URTEC-3859049-MS. https://doi.org/10.15530/urtec-2023-3859049

Yu, W., Lashgari, H. R., Wu, K., and Sepehrnoori, K. 2015. CO_2 Injection for Enhanced Oil Recovery in Bakken tight Oil Reservoirs. *Fuel* **159**: 354-363. https://doi.org/10.1016/j.fuel.2015.06.092.

Zhang, H., Sun, S. and Qiao, R. 2022. Molecular Anatomy and Macroscopic Behavior of Oil Extraction from Nanopores by CO_2 and CH_4. *Fuel* **324:** 124662. https://doi.org/10.1016/j.fuel.2022.124662.

Zhang, H., Wang, S., Wang, X., et al. 2024. Enhanced Recovery of Oil Mixtures from Calcite Nanopores Facilitated by CO_2 Injection. *Energy & Fuels* **38**(6): 5172-5182. https://pubs.acs.org/doi/10.1021/acs.energyfuels.3c05235.

Zhang, W., Feng, Q., Wang, S., et al. 2021. CO_2-regulated Octane Flow in Calcite Nanopores from Molecular Perspectives. *Fuel* **286:** 119299. https://doi.org/10.1016/j.fuel.2020.119299.

Zhu, Z. 2020. Selective Hindrance during Oil Flow through Nanoporous Shale Rocks. PhD dissertation, Colorado School of Mines, Golden, Colorado (December 2020).

Zhu, Z., Coskuner, Y., Yin, X., and Ozkan, E. 2020b. Experimental and Molecular Studies of the Effect of CO_2 on Hindered Flows of Oil through Niobrara Shale. Paper presented at the SPE/AAPG/SEG Unconventional Resources Technology Conference, Austin, Texas, USA, 20–22 July. URTEC-2020-3088-MS. https://doi.org/10.15530/urtec-2020-3088.

Zhu, Z., Fang, C., Qiao, R., Yin, X., and Ozkan, E. 2019. Experimental and Molecular Insights on Sieving of Hydrocarbon Mixtures in Niobrara Shale. Paper presented at the SPE/AAPG/SEG Unconventional Resources Technology Conference, Denver, Colorado, USA, 22-24 July. URTEC-2019-69-MS. https://doi.org/10.15530/urtec-2019-69.

Zhu, Z., Fang, C., Qiao, R., Yin, X., and Ozkan, E. 2020a. Experimental and Molecular Insights on Mitigation of Hydrocarbon Sieving in Niobrara Shale by CO_2 Huff 'n' Puff. *SPE J.* **25** (4): 1803–1811. SPE-196136-PA. https://doi.org/10.2118/196136-PA